Anderson model and then performing the Schrieffer-Wolff transformation (see Ref. 6) a conduction-electron–lattice relaxation may contribute to the localized-moment-lattice relaxation in the transformed Hamiltonian (unpublished).

[6]R. J. Schrieffer and P. A. Wolff, Phys. Rev. 149, 491 (1966).

[7]J. Kondo, Progr. Theoret. Phys. (Kyoto) 28, 846 (1962).

[8]The assumption made here is in agreement with the result of Ref. 6.

[9]L. D. Landau and E. M. Lifshitz, *Quantum Mechanics* (Pergamon, New York, 1965).

[10]The application of Feynman diagrams to spin-dependent interactions is not generally justified owing to the different spin factors for the different time-ordered diagrams. In second order in H_{sd} and without external magnetic field, the spin factors for the different time-ordered diagrams are the same, and therefore Feynman diagrams can be used. In the presence of a strong external magnetic field, however, where $\langle M \rangle$ cannot be neglected compared to $S(S+1)$, even in second order in H_{sd} Feynman diagrams cannot be applied.

[11]Further discussion of this approximation can be found in the Appendix of Ref. 13.

[12]A. A. Abrikosov, Physics 2, 5 (1965).

[13]F. Mezei and A. Zawadowski (unpublished).

[14]J. Sólyom and A. Zawadowski, Physik Kondensierten Materie 7, 325 (1968); 1, 342 (1968).

[15]H. Suhl, Phys. Rev. 138, A515 (1965).

[16]W. Brenig and W. Götze, Z. Physik 217, 188 (1969).

[17]A. Zawadowski and P. Fazekas, Z. Physik 226, 235 (1969).

[18]See Eqs. (18) and (24).

[19]A. Zawadowski and P. Fazekas, J. Appl. Phys. (to be published).

[20]M. D. Daybell and W. A. Steyert, Phys. Rev. Letters 20, 195 (1968).

[21]M. D. Daybell, W. P. Pratt, Jr., and W. A. Steyert, Phys. Rev. Letters 22, 401 (1969).

[22]P. Fazekas and A. Zawadowski (unpublished).

[23]The definition of T_{eff} can be found in Refs. 3 and 4.

[24]This result is proved by Abrikosov (see Ref. 12) and corresponds to a unitarity condition.

PHYSICAL REVIEW B VOLUME 3, NUMBER 1 1 JANUARY 1971

Raman Scattering in $CsMnF_3$ †

S. R. Chinn

Lincoln Laboratory, Massachusetts Institute of Technology, Lexington, Massachusetts 02173

(Received 17 August 1970)

We have observed Raman scattering from the antiferromagnet $CsMnF_3$ over the temperature range from 5 to 300 °K. Of the 33 predicted Raman active normal modes, at low temperature, we have observed and identified 29, belonging to the A_{1g}, E_{1g}, and E_{2g} representations of the space group D_{6h}^4. At higher temperatures many of these lines broadened and shifted in energy from anharmonic interactions. Below the antiferromagnetic ordering temperature 53.5 °K, we have also seen Raman scattering from a two-magnon excitation located at 92.8 cm^{-1} at 5 °K. The energy of this line is consistent with the prediction of spin-wave modes calculated using previously determined excnange constants.

I. INTRODUCTION

The compound $CsMnF_3$ is a transparent antiferromagnet ($T_N = 53.5$ °K)[1] which belongs to the hexagonal space group D_{6h}^4. In this structure, shown in Fig. 1, there are 30 atoms or six formula units in the unit cell in both the paramagnetic and antiferromagnetic phases. This compound is different in its structure and properties from the chemically similar perovskites such as $RbMnF_3$ and $KMnF_3$, and is isomorphic with $RbNiF_3$ and the hexagonal modification of $BaTiO_3$. Much recent work, particularly concerning the magnetic and optical properties, has been carried on $CsMnF_3$, including NMR,[1–4] optical absorption,[5,6] and magnetoelastic interaction studies.[7] This paper reports on phonon and two-magnon excitations which were observed in $CsMnF_3$ by means of Raman scattering.

Before continuing with the results of the present experiment and their interpretation, we shall briefly summarize the most important features of the $CsMnF_3$ structure. In their antiferromagnetically ordered state, the spins of the Mn^{2+} ions ($S=\frac{5}{2}$) lie in the basal plane in alternate antiparallel layers.[1] In addition to the negative uniaxial anisotropy, there is also a very small basal plane anisotropy having sixfold symmetry. Examination of the crystal structure shows that there are two different types of sites for the Mn^{2+} ions. One type, labeled A, is in a slightly distorted octahedron of F^- ions which shares only corners with other $6F^-$-Mn^{2+} octahedra. The second type of site, labeled B, is in an octahedron which shares three corners with A-site octahedra and a common face with another B-site octahedron. As in $RbNiF_3$,[8] this structure gives rise to two types of superexchange paths, one with an approximately 180° angle, for the Mn_A-F-Mn_B bond, and the other, about 90°, for the Mn_B-F-Mn_B bond. In $CsMnF_3$, both of these interactions are antiferromagnetic.

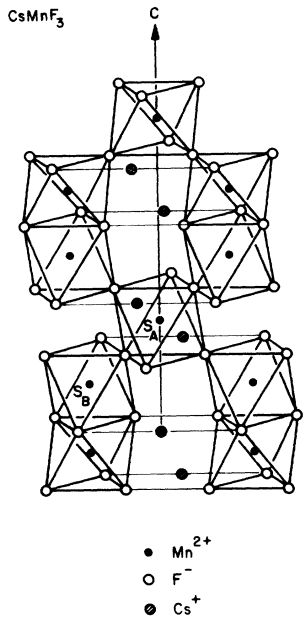

FIG. 1. Crystal structure of $CsMnF_3$.

Of the 90 phonon normal modes, 33 are allowed by symmetry to be Raman active. In the present work we have experimentally observed 29 of these at low temperatures, and have examined the Raman spectrum from 5 to 300 °K. At low temperatures we have also seen a weak Raman line arising from two magnons. Its temperature dependence is similar to that observed in other antiferromagnets. In addition, there is a large degree of anharmonic elastic interactions which causes a noticeable shift and broadening of some of the observed phonon lines as the temperature is increased.

II. EXPERIMENT

Three samples of $CsMnF_3$ were kindly lent to us by Dr. M. Seavey of the Air Force Cambridge Research Laboratory. After polishing, the largest was about $2\times3\times3$ mm, and the other two samples, which were from a different boule, were slightly smaller. Of the two smaller samples, one had been annealed, but all three samples exhibited the same degree of intense fluorescence in the red-orange region at low temperatures, presumably arising from defects or impurities. The largest sample showed the best Laue x-ray patterns, and only the small unannealed sample gave evidence of slight polycrystallinity when viewed with a polariscope to check the c-axis orientation. Identical Raman spectra were observed with all three samples.

The Raman scattering measurements were carried out in standard fashion using 4880-Å polarized radiation from an argon ion laser. Separate fluorescence spectra from the laser were obtained in order to distinguish the Raman lines from fluorescence contributions. We also verified the Raman spectra using the argon laser line at 5145 Å, which, however, yielded slightly lower signal-to-noise ratios. The laser power was varied from 75 to 400 mW, with the lower power being used at high temperatures to minimize sample heating and prevent damage. Consequently, the signal-to-noise ratio was better at low temperatures, although the temperature dependence of the Raman lines also contributed to this effect. The samples were fastened to a cold finger in a variable temperature Dewar, in which the temperature was maintained by regulating the flow of cold helium gas around the sample mount and varying the electrical power applied to sample mount heaters in a feedback-controlled network. The measurement and control thermometers were calibrated Ge and Pt resistances, and temperatures were typically stabilized to ± 0.5 °K. The laser beam was focused and transmitted through the sample, and the scattered radiation was collected in a direction 90° from the beam and focused onto the entrance slit of a double-grating spectrometer. A half-wave plate in the laser beam and a polarizing prism before the spectrometer slit were used to vary the incident and detected scattered radiation. The analyzed radiation from the spectrometer was detected by a cooled photomultiplier tube having an S-20 cathode surface. The photoelectron pulses from the tube were amplified and counted, and were also filtered to provide an analog signal to a chart recorder, which was driven as the spectrometer wavelength was swept.

III. RAMAN SCATTERING FROM PHONONS

As mentioned above, $CsMnF_3$ belongs to the space group D_{6h}^4 and is isomorphic with $RbNiF_3$, whose phonon spectrum has been studied by Fleury *et al.*[9] Since these two compounds have identical crystallographic symmetry (as far as corresponding site locations are concerned, but not for spin orientations), we can make direct use of the group-theoretical results found for $RbNiF_3$[9] in determining the allowed Raman modes. There are

$$5A_{1g} + 2A_{2g} + 1A_{1u} + 7A_{2u} + 6B_{1g} + 1B_{2g} + 2B_{1u} + 6B_{2u} + 6E_{1g} + 8E_{2g} + 9E_{1u} + 7E_{2u}$$

total phonon representations. Of these, $5A_{1g}$ (nondegenerate) and $6E_{1g} + 8E_{2g}$ (doubly degenerate) modes are allowed to be Raman active. The scattering tensors for these modes are[10]

$$\begin{bmatrix} a & 0 & 0 \\ 0 & a & 0 \\ 0 & 0 & b \end{bmatrix} \quad \begin{bmatrix} 0 & 0 & 0 \\ 0 & 0 & c \\ 0 & c & 0 \end{bmatrix} \quad \begin{bmatrix} 0 & 0 & -c \\ 0 & 0 & 0 \\ -c & 0 & 0 \end{bmatrix} \quad \begin{bmatrix} 0 & d & 0 \\ d & 0 & 0 \\ 0 & 0 & 0 \end{bmatrix} \quad \begin{bmatrix} d & 0 & 0 \\ 0 & -d & 0 \\ 0 & 0 & 0 \end{bmatrix},$$

A_{1g} E_{1g} E_{1g} E_{2g} E_{2g}

where the tensor Cartesian coordinates refer to the incident and scattered radiation polarization components in the crystallographic reference system (z parallel to the c axis).

These modes could be distinguished experimentally by selection of the incident and scattered polarizations for various crystal orientations. In some cases, because of small misalignments, small polarization ellipticity, internal reflections, and the size of optical collection angle, strong Raman lines appeared weakly in forbidden polarizations. Some typical spectra are shown in Fig. 2 for $xx+xy$ and xz polarizations at 5 °K. Shown on the spectra of Fig. 2 below some of the lines are stars which indicate luminescence lines from the argon laser or circles which indicate Raman lines appearing in forbidden polarization. The experimental results taken at a sample temperature of 5 °K are summarized in Table I. A qualitative estimate of the relative amplitudes is indicated by very strong (VS), strong (S), medium (M), weak (W), and very weak (VW), where each strength is roughly a factor of 2 weaker than the preceding one. The small amounts of forbidden polarization lines which appeared (and could be readily identified) are not indicated in the table. Some of the different symmetry modes were so close together that they could not be resolved when scattering from both types of representations was allowed. The presence of two separate modes was established by examining configurations when only one such mode at a time was allowed. Small differences in peak locations were found, and, more important, it was verified that the intensities of the representations intended to be suppressed were indeed small. At low temperatures the phonon lines were quite narrow, on the order of the instrumental resolution which was ~3 cm^{-1} with the narrowest practical slits. As the temperature was increased most of the lines broadened noticeably and underwent slight shifts in frequency. Some typical spectra at 300 °K for the same configurations as in Fig. 2 are shown in Fig. 3. A striking change occurred in the most intense observed line, an A_{1g} mode with energy of 387.7 cm^{-1}, at 5 °K. Its behavior was typical of several other lines, such as the E_{2g} mode at 276.6 cm^{-1}, and we have ex-

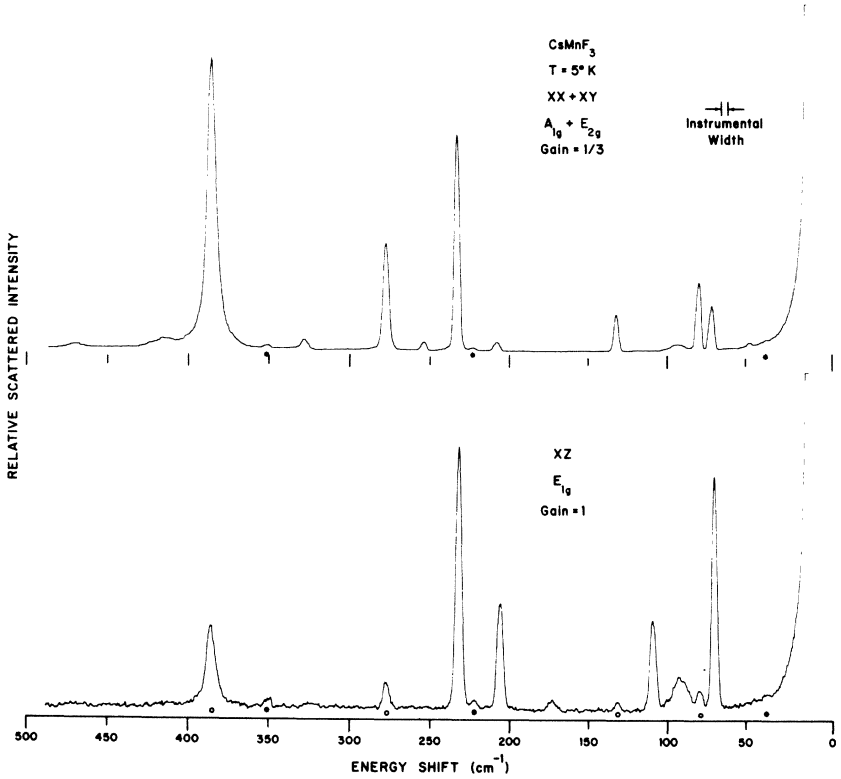

FIG. 2. Raman spectra of $CsMnF_3$ at 5 °K.

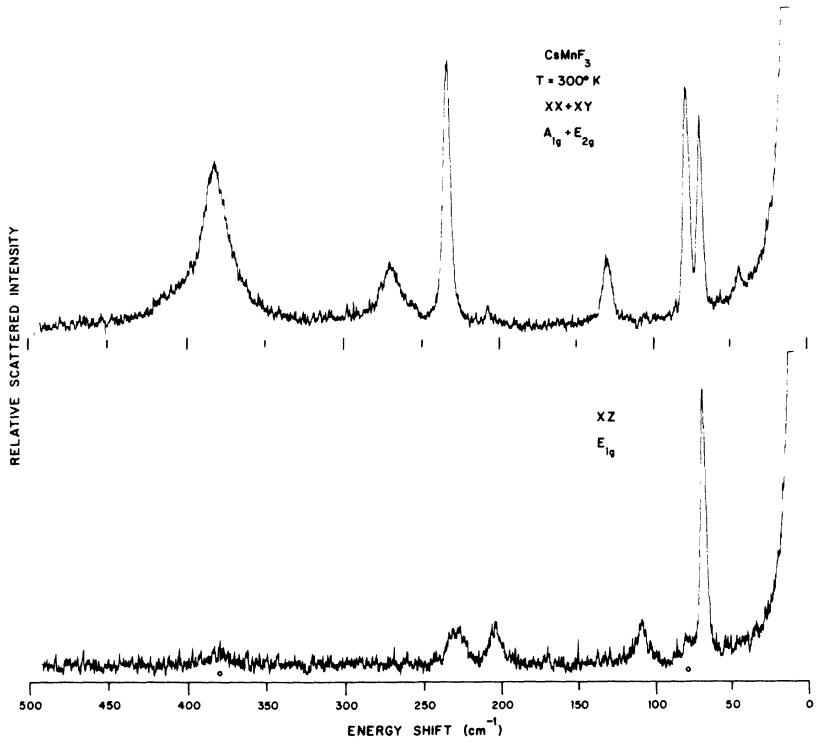

FIG. 3. Raman spectra of $ScMnF_3$ at 300 °K.

TABLE I. Experimentally observed Raman active phonons in $CsMnF_3$ at 5 °K.

Representation	Frequency (cm^{-1})	Polarization	Relative amplitude (at 5 °K)
A_{1g}	70.7	xx, zz	M, S
A_{1g}	253.9	xx, zz	W, VW
A_{1g}	387.7	xx, zz	VS, VS
A_{1g}	413.3	xx, zz	VW, W
A_{1g}	469.6	xx, zz	VW, W
E_{1g}	69.6	xz	S
E_{1g}	109.3	xz	M
E_{1g}	172.7	xz	VW
E_{1g}	205.0	xz	M
E_{1g}	231.6	xz	S
E_{2g}	46.7	xy	VW
E_{2g}	79.6	xy	S
E_{2g}	130.8	xy	M
E_{2g}	207.2	xy	W
E_{2g}	233.2	xy	VS
E_{2g}	276.6	xy	S
E_{2g}	327.4	xy	W

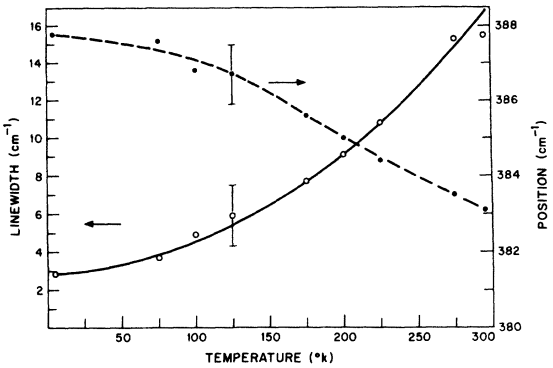

FIG. 4. Raman shift and linewidth (full width half-maximum) for most intense A_{1g} mode in $CsMnF_3$ as a function of temperature.

amined in greater detail the temperature dependence of the Raman shift and linewidth for this most intense A_{1g} mode. The results of position and linewidth (full width half-maximum) measurements from 5 to 300 °K are shown in Fig. 4. We have determined the approximate linewidths by subtracting the measured linewidth of the spectrometer response ($2.8\ cm^{-1}$ with 100-μ slit openings) from the linewidths of the recorded Raman spectra. Because of nonlinearities and inconsistency in the spectrometer drive, the absolute energy shifts are accurate only to $\pm 1\ cm^{-1}$.

It is difficult to formulate a quantitative explanation for this temperature dependence since so little is known about the total phonon spectrum of $CsMnF_3$, particularly the energies of the non-Raman active phonons and the dispersion of any of the phonon energies. The general theoretical results for the effects of anharmonic interactions on the phonon en-

ergy shifts and linewidths, as found from Green's-function theory, have been successfully applied in the study of α quartz by Pine and Tannenwald.[11] In the present case, a very crude fit to the data can be obtained by suitable combinations of Bose factors for $\vec{k} = 0$ Raman active phonons with which the broadened modes might interact. However, this is an *ad hoc* unsatisfactory procedure in view of the lack of knowledge of the other phonon energies. It can be said that the relative amounts of shifts and broadening in $CsMnF_3$ are at least consistent with expected Bose population factors. It is interesting that in the isomorphic compound $RbNiF_3$, all of the Raman lines observed by Fleury *et al.*[9] were less than a few cm^{-1} wide, even up to 300 °K.

IV. RAMAN SCATTERING FROM MAGNONS

Along with the phonon lines observed in the Raman spectra, we have also seen a relatively weak broad line with peak location at 92.8 cm^{-1}. This line broadened further and its peak shifted to lower energies as the temperature was increased from 5 °K, and at 50 °K was quite difficult to observe. This excitation was seen in all scattering configurations with little change in intensity, and did not obey any of the polarization selection rules for phonons. From its position, breadth, temperature dependence, and polarization properties, it seems clear that this line arises from Raman scattering by two magnons.

It was difficult to follow the exact position and breadth of the two-magnon line as a function of temperature because of its weak scattering cross section, its small energy shift which put it close to the tail of the elastically scattered laser radiation, and its proximity to several phonon lines, not all of which could be discriminated against. For these reasons we have indicated the qualitative two-magnon scattering behavior in Fig. 5 with spectra recorded at several temperatures. The relative strength of the two-magnon spectrum relative to the A_{1g} and E_{2g} phonons of Fig. 5, as well as to the E_{1g} phonons, can be seen in Fig. 2, where the two-magnon line appears just to the right of the 100-cm^{-1} mark. It is apparent that the temperature dependence of this line is much more rapid than that associated with the phonons. The two-magnon spectra observed in other antiferromagnets[12,13] exhibited a similar shift and broadening, and also persisted at temperatures above the Néel temperature. In $CsMnF_3$, this behavior is at least approximately maintained, although at T_N we could not distinguish the presence of the two-magnon line from the large background.

Interpretation of the low-temperature magnon scattering in a qualitative fashion is as difficult as in the case of $RbNiF_3$,[8] because of the complex nature of the magnon dispersion relations. Even in

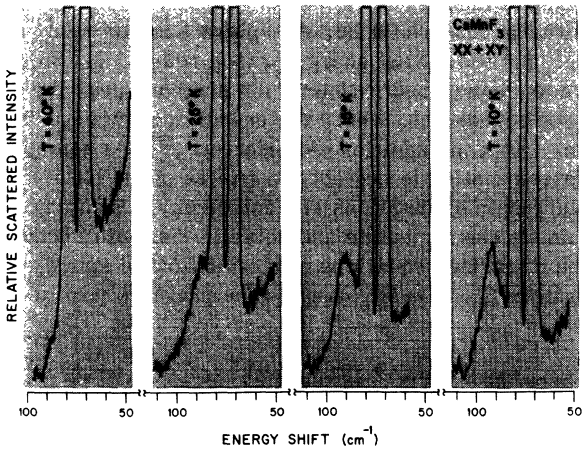

FIG. 5. Two-magnon Raman spectra in $CsMnF_3$ as a function of temperature .

the simplest approximation, neglecting anisotropy, dipolar, and hyperfine interactions, there are three doubly degenerate spin-wave branches in the one-magnon dispersion relations. While these wave-vector-dependent energies can be found as solutions to a cubic equation, it is a rather difficult task to evaluate analytically, or even numerically, quantities such as the perfect crystal magnon Green's functions, which are necessary if effects like the magnon-magnon interaction are to be included exactly in the scattering analysis. This effect plays an important part in understanding Raman scattering from two magnons, since the dominant radiation interaction causing the scattering from spin excitations is assumed to be an interionic exchange mechanism between adjacent antiparallel spins. This pair excitation process has the effect of altering the line shape and shifting the peak to lower energy by an amount roughly equal to the exchange constant.[14] Without treating the scattering in an exact fashion, we may approximate the results by considering the scattering to arise from the $\vec{k} = 0$ excitation of two noninteracting magnons with equal and opposite wave vectors lying near the Brillouin zone edge where the density of states is highest. This corresponds to an Ising model, and in this limit, the binding energy arising from the proximity of the nearest-neighbor spin excitations is also equal to the exchange constant between the excited spins.

Before continuing with the discussion of Raman scattering, we shall briefly review the main features of the single-magnon modes in $CsMnF_3$. The model

which is used to compute these modes is that of an isotropic-exchange antiferromagnet, having exchange constant J_{AB} between nearest A- and B-site spins, and J_{BB} between nearest B-site spins. Although $CsMnF_3$ does have easy plane anisotropy, with $K_1/M = -7500$ Oe,[1] this plays a major role only for the lowest energy branch near $\vec{k}=0$. Since we are concerned with only the magnons near the zone boundaries, where the energies change ± 0.7 cm^{-1} with the addition of anisotropy,[15] it is a good approximation to neglect the effects of the basal plane spin orientations and anisotropy. By doing this we can formulate and solve in a simple manner the linearized equations of motion for the spin operators $S_l^+ = S_l^x + iS_l^y$, as was done previously in investigating the garnets[15] and $RbNiF_3$.[8] Using the relation

$$i\dot{S}_l^+ = [S_l^+, \mathcal{H}] \quad (\hbar = 1) \ , \tag{1}$$

where $\mathcal{H}$ is the Heisenberg exchange Hamiltonian, we find

$$\omega S_l^+ = S_l^+ \textstyle\sum_j J_{lj} \langle S_j^z \rangle_0 - \langle S_l^z \rangle_0 \sum_j J_{lj} S_j^+ \ , \tag{2}$$

where a time dependence $e^{i\omega t}$ has been assumed for the normal modes. At zero temperature, we assume $\langle S^z \rangle_0 = \pm \frac{5}{2}$, the sign depending on the sublattice. Using the $CsMnF_3$ lattice, after spatial Fourier decomposition, we obtain the secular equation of the normal modes

$$A = \omega I \ , \tag{3}$$

where the matrix A is given by

$$A = \begin{bmatrix} -J_{BB} - 3J_{AB} & -J_{BB} & 0 & 0 & 0 & -J_{AB} e^{ik_z c} \xi \\ J_{BB} & +J_{BB} + 3J_{AB} & 0 & 0 & J_{AB}\xi & 0 \\ 0 & 0 & +J_{BB} + 3J_{AB} & J_{BB} & J_{AB}\zeta & 0 \\ 0 & 0 & -J_{BB} & -J_{BB} - 3J_{AB} & 0 & -J_{AB}\zeta \\ 0 & -J_{AB}\xi^* & -J_{AB}\zeta^* & 0 & -6J_{AB} & 0 \\ J_{AB} e^{-ik_z c}\xi^* & 0 & 0 & J_{AB}\zeta^* & 0 & 6J_{AB} \\ S_{B_1} & S_{B_2} & S_{B_3} & S_{B_4} & S_{A_1} & S_{A_2} \end{bmatrix} . \tag{4}$$

The factors in Eq. (4) are defined as follows:

$$\xi = 1 + e^{ik_x a} + e^{ik_x a/2 + ik_y a\sqrt{3}/2} \ ,$$

$$\zeta = 1 + 2\cos(k_x a/2)\, e^{ik_y a\sqrt{3}/2} \ ,$$

and the stars denote complex conjugates. Using the values $J_{AB} = 3.53$ cm^{-1} and $J_{BB} = 3.71$ cm^{-1} determined by Seavey,[7] we have numerically computed the magnon dispersion relations shown in Fig. 6 for three different directions of $\vec{k}$ in the Brillouin zone. Some of these were also computed by Seavey[16] using a canonical transformation technique with linearized spin-excitation operators, but the present method has the slight advantage of giving more physical insight from the equations of motion and giving a very simple picture of the eigenmodes, as well as energies, for certain points in the Brillouin zone. The magnon normal modes and energies are nearly the same over the six side faces of the zone, and can be approximately characterized by the $\vec{K}$-point solutions, which are particularly simple. At $\vec{k} = \vec{K}$, the upper branch energy is $E_+ = 6J_{AB}$ and the spin excitations are completely on the A sites. The two lower branches, which are degenerate at the $\vec{K}$ point, have energy $E_- = [3J_{AB}(3J_{AB} + 2J_{BB})]^{1/2}$, and the excitations are entirely on the B-site spins. Although we have not computed the magnon density of states, the dispersion relation analysis shows

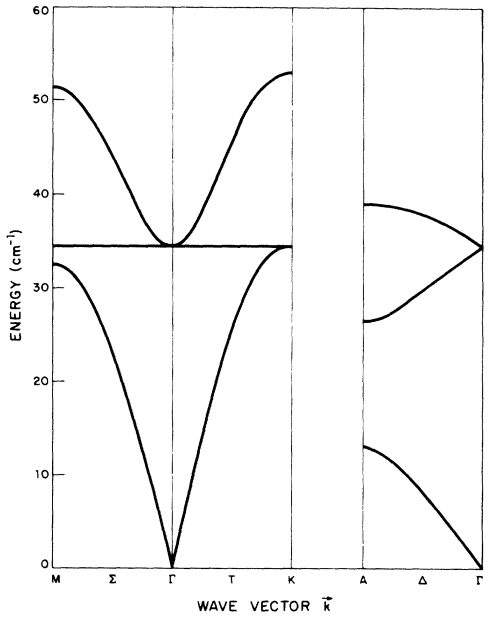

FIG. 6. One-magnon dispersion relations in $CsMnF_3$ calculated using $J_{AB} = 3.53$ cm^{-1} and $J_{BB} = 3.71$ cm^{-1} with no anisotropy.

that the magnon branches are flat and maintain approximately the same energies over a large volume near the zone edge sides, leading to peaks at these energies near E_+ and E_-. In contrast, the $\vec{A}$-point energies are much lower, and are a distinct minimum on the top and bottom horizontal zone faces.

This analysis leads to a rather simple explanation of the two-magnon scattering results. One pair of magnons consisting of an upper branch excitation near the $\vec{K}$ or $\vec{M}$ point and a lower branch magnon with opposite wave vector fulfills the conditions assumed in the Raman scattering mechanism and is located at a peak in the joint density of states. The pair excitation interaction, of the form $\sum_{ij} B_{ij} \vec{S}_i \cdot \vec{S}_j$, has been consistent with all the observations of two-magnon Raman scattering in MnF_2,[17] FeF_2,[17] $RbMnF_3$,[18] NiF_2,[19] and $RbNiF_3$.[8,9] With this type of scattering interaction, the magnon branches, having high densities of states and able to give rise to second-order Raman scattering, have energies $\sim E_+$ and $\sim E_-$ and are on the A and B lattices, respectively. Notice that the combination of two upper-branch or two lower-branch zone edge magnons would not be favorable for scattering since these pairs would be almost completely restricted to the A or B lattices, respectively, contrary to the assumption of neighboring antiparallel spins being excited.

It is this same assumption which also leads to the nonnegligible effects of magnon-magnon interactions in the Raman scattering process. In the Ising model, which corresponds to the flat-band approximation used above, it is easy to see that the effect of having two neighboring spins simultaneously excited is to lower the total excitation energy by the amount of their exchange interaction constant. More detailed Green's-function calculations[14,20] have shown that this is a good approximation when the true density of states has a single narrow peak. Since the unperturbed joint density of states for allowed pairs of magnons in $CsMnF_3$ seems to have a sharp peak near $E_+ + E_-$, this approximation is probably valid. Therefore, in lieu of a more exact calculation, the simplest estimate is for the two-magnon Raman peak to have an energy

$$E_{\mathrm{RAM}} = 6J_{AB} + [3J_{AB}(3J_{AB} + 2J_{BB})]^{1/2} - J_{AB} \ .$$

Using the previously given values of the exchange constants we find $E_{\mathrm{RAM}} = 84\ \mathrm{cm}^{-1}$. This is compared with the experimental location of the peak at $92.8 \pm 1.0\ \mathrm{cm}^{-1}$. Although there is some experimental error arising from the large linewidth, low signal-to-noise ratio, and spectrometer calibration uncertainty, our value for E_{RAM} is greater than the theoretical prediction. However, the calculations have neglected anisotropy energies as well as further neighbor interactions which could increase the predicted energies by several cm^{-1}. A possible explanation of the remaining error lies in the uncertainty of various parameters used to estimate the exchange constants. The magnon-phonon interaction measurements performed by Seavey[7,16] gave a value of the parameter

$$\alpha = 0.85 \pm 0.03 \times 10^{-4}\ \mathrm{Oe}^2\mathrm{cm}^2 \ ,$$

where

$$\alpha = [(2R+1)/27R]\, a^2 H_E^{\,2} \ , \quad R = J_{BB}/3J_{AB} \ ,$$

$a = 6.213$ Å = transverse unit-cell dimension,[21]

$H_E = 0.35 \times 10^6$ Oe = exchange field.[1]

In addition, H_E, which was found from susceptibility measurements, could be in error by several percent, particularly in view of other values found, ranging from 0.31×10^6 to 0.33×10^6 Oe.[3,4] With $\alpha = 0.88 \times 10^{-4}\ \mathrm{Oe}^2\mathrm{cm}^2$ and $H_E = 0.33 \times 10^6$ Oe, the two-magnon Raman energy becomes $E_{\mathrm{RAM}} \simeq 90.6\ \mathrm{cm}^{-1}$, which is quite close to the observed value, particularly in view of the simplifications used in the spin-wave and scattering models.

V. CONCLUSION

We have observed all but four of the 33 Raman active phonon modes allowed by symmetry. In terms of the D_{6h}^4 space group representations, these were divided into five (out of five allowed) singly degenerate A_{1g} modes, five (out of six allowed) doubly degenerate E_{1g} modes, and seven (out of eight allowed) doubly degenerate E_{2g} modes. They were identified by their polarization selection rules determined from group theory. The phonon behavior in $CsMnF_3$ provides an interesting contrast to its isomorph $RbNiF_3$, since the anharmonic interactions in the former are so much larger. Perhaps a more detailed examination of corresponding vibrations can provide some insight into the lattice potentials of these two materials. Of course, much more information is needed on all of the phonon modes throughout the Brillouin zone before the phonon interactions can be treated in a quantitative fashion.

As far as the magnetic scattering is concerned, there are fewer unanswered questions in $CsMnF_3$ than in $RbNiF_3$. Because the 90° Ni_B-F-Ni_B interaction in $RbNiF_3$ is ferromagnetic, the spin ordering is with all the B-site spins parallel, and antiparallel to the A-site spins, with a resultant net moment in the ferrimagnetic ground state. One strong two-magnon Raman line was observed in this material. $RbNiF_3$ has six magnon modes and from the dispersion relations and mode analysis[8] at least one other two-magnon line might be expected, but was not seen. In $CsMnF_3$, however, only one peak is predicted and was observed, coming from opposite upper- and lower-branch magnons at the transverse Brillouin zone edge. The observed energy is

also consistent, if not in precise agreement, with the value calculated from previously determined exchange constants. No interaction effects between the magnons and $\vec{k}=0$ Raman active phonons were seen, although such coupling might be expected. Also, since the crystallographic cell remains the same above and below T_N, no symmetry changes affecting the phonon spectrum were seen. Although not observed in our experiments, it should be possible to see single $\vec{k}=0$, one-magnon Raman scattering. This would take place by a different means from the two-magnon process, probably by spin-orbit interactions as opposed to a pair exchange interaction with the radiation fields. The one-magnon scattering could therefore be much weaker, and its low expected energy, $\sim 6.7\ \mathrm{cm}^{-1}$ from the acoustic branch[16] or $\sim 35\ \mathrm{cm}^{-1}$ from the optic branch, would put it on a large background signal of elastically scattered laser radiation.

ACKNOWLEDGMENTS

The author is grateful to Dr. M. Seavey for kindly lending samples of $CsMnF_3$ and for detailed discussions concerning his work on this compound. Thanks are expressed to Dr. G. Wright for helpful criticism of this manuscript, and to him and Dr. A. Pine for fruitful conversations about phonon interactions.

[1] K. Lee, A. M. Portis, and G. L. Witt, Phys. Rev. 132, 144 (1963).
[2] G. L. Witt and A. M. Portis, Phys. Rev. 136, A1316 (1964).
[3] V. Minkiewicz and A. Nakamura, Phys. Rev. 143, 361 (1966).
[4] L. B. Welsh, Phys. Rev. 156, 370 (1967).
[5] R. Stevenson, Can. J. Phys. 44, 3269 (1966).
[6] F. Saito, Solid State Commun. 8, 969 (1970).
[7] M. H. Seavey, Phys. Rev. Letters 23, 132 (1969).
[8] S. R. Chinn and H. J. Zeiger, Phys. Rev. Letters 21, 1589 (1968). S. R. Chinn, H. J. Zeiger, and J. R. O'Connor (unpublished).
[9] P. A. Fleury, J. M. Worlock, and H. J. Guggenheim, Phys. Rev. 185, 738 (1969).
[10] R. Loudon, Advan. Phys. 13, 423 (1964).
[11] A. S. Pine and P. E. Tannenwald, Phys. Rev. 178, 1424 (1969).
[12] P. A. Fleury, J. Appl. Phys. 41, 886 (1970).
[13] S. R. Chinn, H. J. Zeiger, and J. R. O'Connor, J. Appl. Phys. 41, 894 (1970).
[14] R. J. Elliott and M. F. Thorpe, J. Phys. C 2, 1630 (1969).
[15] A. Brooks Harris, Phys. Rev. 132, 2398 (1963).
[16] M. H. Seavey, Ph.D. thesis, Harvard University, 1970 (unpublished).
[17] P. A. Fleury and R. Loudon, Phys. Rev. 166, 514 (1968).
[18] P. A. Fleury, Phys. Rev. Letters 21, 151 (1968).
[19] P. A. Fleury, Phys. Rev. 180, 591 (1969).
[20] M. F. Thorpe, J. Appl. Phys. 41, 892 (1970).
[21] A. Zalkin, K. Lee, and D. H. Templeton, J. Chem. Phys. 37, 697 (1962).

†Work sponsored by the Department of the Air Force.

PHYSICAL REVIEW B VOLUME 3, NUMBER 1 1 JANUARY 1971

Spin Dependence of the Neutron-Capture Cross Section of Vanadium and the Internal Magnetic Field at Vanadium Nuclei*

H. Postma, † L. Vanneste, ‡ and V. L. Sailor
Brookhaven National Laboratory, Upton, New York 11973
(Received 24 June 1970)

The spin dependence of the neutron-capture cross section of vanadium at 0.115 eV has been measured with the aid of polarized neutrons and polarized vanadium nuclei. It is concluded that the capture cross section of V^{51} is mainly related to spin $J=I-\frac{1}{2}$. In addition, it is shown that the internal field at the vanadium nuclei is less than 4 kOe in very pure vanadium, which apparently does not become ferromagnetic down to 0.06 K.

Transmission experiments with polarized neutrons through a target of polarized vanadium nuclei were carried out at the High Flux Beam Reactor at Brookhaven. Polarized neutrons of 0.115 eV were obtained with the aid of the high-precision crystal spectrometer using (111) reflection from a magnetized 92% Co-8% Fe single crystal.[1] Second-order reflected neutrons were removed from the beam using an erbium filter. Vanadium nuclei were polarized at temperatures between 0.05 and 4.2 K using a magnetic field up to 50 kOe generated with the aid of a superconducting split solenoid. Temperatures below 0.85 K were obtained by adiabatic demagnetization of a chrome-potassium-alum salt assembly thermally connected to the sample. The vanadium sample (10.3 mm thick) and indium (3.35 mm thick) were soldered between two strips of copper, which were connected to the salt assem-

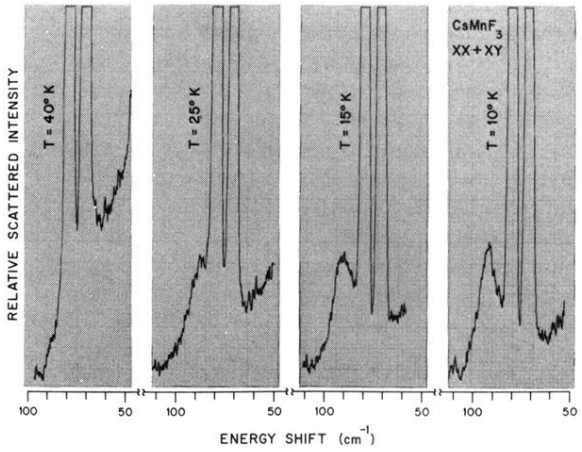

FIG. 5. Two-magnon Raman spectra in $CsMnF_3$ as a function of temperature .